Journal of Theoretical Biology 454 (2018) 11–21

Contents lists available at ScienceDirect

Journal of Theoretical Biology

journal homepage: www.elsevier.com/locate/jtbi

Dependence of absence seizure dynamics on physiological parameter evolution

F. Deeba[a,b,*], Paula Sanz-Leon[a,b], P. A. Robinson[a,b]

[a] School of Physics, University of Sydney, NSW 2006, Australia
[b] Center for Integrative Brain Function, University of Sydney, NSW 2006, Australia

ARTICLE INFO

Article history:
Received 12 February 2018
Revised 22 May 2018
Accepted 24 May 2018
Available online 25 May 2018

ABSTRACT

A neural field model of the corticothalamic system is applied to investigate the temporal and spectral characteristics of absence seizures in the presence of a temporally varying connection strength between the cerebral cortex and thalamus. Increasing connection strength drives the system into an absence seizure-like state once a threshold is passed and a supercritical Hopf bifurcation occurs. The dynamics and spectral characteristics of the resulting model seizures are explored as functions of maximum connection strength, time above threshold, and the rate at which the connection strength increases (ramp rate). Our results enable spectral and temporal characteristics of seizures to be related to changes in the underlying physiological evolution of connections via nonlinear dynamics and neural field theory. Spectral analysis reveals that the power of the harmonics and the duration of the oscillations increase as the maximum connection strength and the time above threshold increase. It is also found that the time to reach the stable limit-cycle seizure oscillation from the instability threshold decreases with the square root of the ramp rate.

1. Introduction

Epileptic seizures involve intense, abnormal, synchronous neural firing in the corticothalamic system (Browne and Holmes, 2000; Coombes and Terry, 2012; Engel and Pedley, 1997; Hall and Kuhlmann, 2013; Jirsa et al., 2017; Kim et al., 2009; Kramer et al., 2012; Larter et al., 1999; Liley and Bojak, 2005; Lytton, 2008; Lytton et al., 2005; Penfield, 1933; Robinson et al., 2002; Salek-Haddadi et al., 2006; Schiff, 2012; Velazquez et al., 2006; Wendling et al., 2005). Absence seizures are generalized epileptic seizures, most commonly observed in children (Crunelli and Leresche, 2002; Engel and Pedley, 1997; Proix et al., 2014; Suffczynski et al., 2004; 2005; Vercueil et al., 1998), which involve a sudden loss of consciousness, motionless stare, and cessation of ongoing activities (Browne and Holmes, 2000; Engel and Pedley, 1997; Panayiotopoulos, 1999). The majority of absence seizures last for 20 seconds or less (Panayiotopoulos, 1999).

The characteristic hallmark of absence seizure is bilaterally synchronous “spike and wave” discharges (SWDs) with a frequency of 3–4 Hz (Breakspear et al., 2006; Crunelli and Leresche, 2002; Jirsa et al., 2014; Marten et al., 2009; Panayiotopoulos, 1999; Proix et al., 2014; Lopes da Silva et al., 1997; Suffczynski et al., 2004; 2005; Vercueil et al., 1998; Zhao and Robinson, 2015). A number of authors have investigated the mechanism behind SWD generation (Breakspear et al., 2006; Crunelli and Leresche, 2002; Jirsa et al., 2014; Marten et al., 2009; Panayiotopoulos, 1999; Proix et al., 2014; Lopes da Silva et al., 1997; Suffczynski et al., 2004; 2005; Vercueil et al., 1998; Zhao and Robinson, 2015) by using both neural network (Crunelli and Leresche, 2002; Panayiotopoulos, 1999; Proix et al., 2014; Suffczynski et al., 2004; 2005; Vercueil et al., 1998) and neural field approaches (Breakspear et al., 2006; Marten et al., 2009; Zhao and Robinson, 2015). It is widely considered that the transitions from healthy states to spike-wave discharges occur upon changing corticothalamic connectivity strengths, e.g., increasing excitatory connections between the cortex and the thalamus (Breakspear, 2017; Breakspear et al., 2006; Chen et al., 2014; Destexhe, 1999; Dhamala et al., 2004; Guye et al., 2006; Kim and Robinson, 2007; Luo et al., 2012; Marten et al., 2009; Meeren et al., 2002; Roberts and Robinson, 2008; Robinson et al., 2002; Rodrigues et al., 2009; Tan et al., 2007; Ullah et al., 2015; Wallace et al., 2001; Zhao and Robinson, 2015). Thalamic involvement in the SW generation is also supported by in vivo studies (Andrew, 1991; Prevett et al., 1995; Seidenbecher et al., 1998; Steriade et al., 1998; Steriade and Contreras, 1998; Vergnes and Marescaux, 1992; Voss et al., 2009; Williams, 1953).

* Corresponding author at: School of Physics, University of Sydney, NSW 2006, Australia.
E-mail address: farah.deeba@sydney.edu.au (F. Deeba).

https://doi.org/10.1016/j.jtbi.2018.05.029
0022-5193/

Many modeling studies have been done to find the underlying corticothalamic mechanisms of absence seizures (Breakspear et al., 2006; Chen et al., 2014; Marten et al., 2009; Roberts and Robinson, 2008; Robinson et al., 2002; Rodrigues et al., 2009; Yang and Robinson, 2017; Zhao and Robinson, 2015), as well as oscillatory activity during the pre-ictal to ictal transition in the cortex and the thalamus (Berényi et al., 2012; Godlevsky et al., 2006; Liley et al., 1999; van Luijtelaar et al., 2016; Wendling, 2008). However, the impact of underlying parameter changes on the onset and dynamics has not been studied in detail. The possible physiological reasons behind the variation of the amplitudes of the oscillations with time (Breakspear et al., 2006), which are seen in the clinical EEGs like Breakspear et al., are also needed to be explored.

In this study, we apply a widely used neural field model of the corticothalamic system (Breakspear et al., 2006; Kim and Robinson, 2007; Marten et al., 2009; Roberts and Robinson, 2008; Robinson, 2006; Robinson et al., 2002; 2004; Zhao and Robinson, 2015). Neural field theory (NFT) is a continuum approach that predicts the dynamics of large numbers of neurons (Deco et al., 2008; Pinotsis et al., 2012). This model (Freeman, 1975; Jirsa and Haken, 1996; Nunez, 1974; Robinson et al., 1997) has reproduced and unified many observed features of brain activity, including alpha rhythm (O'Connor and Robinson, 2004; Robinson et al., 2003), age-related changes in the physiology of the brain (van Albada et al., 2010), evoked response potentials (Rennie et al., 2002), arousal state (Abeysuriya et al., 2015) dynamics, and many other phenomena as well as enabling estimation of underlying brain parameters by fitting model prediction to data (Abeysuriya et al., 2014a; 2014b; Breakspear et al., 2006; 2003; Chiang et al., 2011; Kim and Robinson, 2007; Marten et al., 2009; Roberts and Robinson, 2008; Robinson, 2006; Robinson et al., 2002; 2004; 2005; 2001; Rodrigues et al., 2006; Zhao and Robinson, 2015). This model has also been used in seizure studies (Breakspear et al., 2006; Kim and Robinson, 2007; Marten et al., 2009; Roberts and Robinson, 2008; Yang and Robinson, 2017; Zhao and Robinson, 2015).

Several studies have demonstrated that a gradual increase of the connection strength between the cortex and thalamus can provoke seizure like dynamics in a NFT model of the corticothalamic system as a result of a supercritical Hopf bifurcation (Breakspear et al., 2006; 2003; Marten et al., 2009; Zhao and Robinson, 2015). However, the dependence of the seizure on the time course of the connection strength has not been studied in detail. In this study, we implement a smooth flat-topped temporal variation function to vary level, duration, and ramp rate to explore the dependence of the seizure dynamics on these parameters. The aims are to understand the effects of physiological parameters, such as, the maximum connection strength, the rate of change of the connection strength, and the time course of the connection strength on the temporal and spectral characteristics of model seizure dynamics, and how the observed dynamics constrain the underlying physiological parameters. We also intend to see the dependence of the amplitude of the model seizure oscillations on these parameters which possibly could lead us to relate the underlying physiological changes to the variation of the amplitude of the oscillations with time seen in clinical EEG (Breakspear et al., 2006).

The outline of this study is as follows: In Section 2 we present the theory of corticothalamic neural field model, in Section 3 we explain the numerical method, in Section 4 we explore the dependence of seizure dynamics on the temporal variation of connection strength, and in Section 5 we give a summary.

2. Theory

In this section we present a brief description of the corticothalamic neural field model, along with the form of temporal variation of corticothalamic coupling strength.

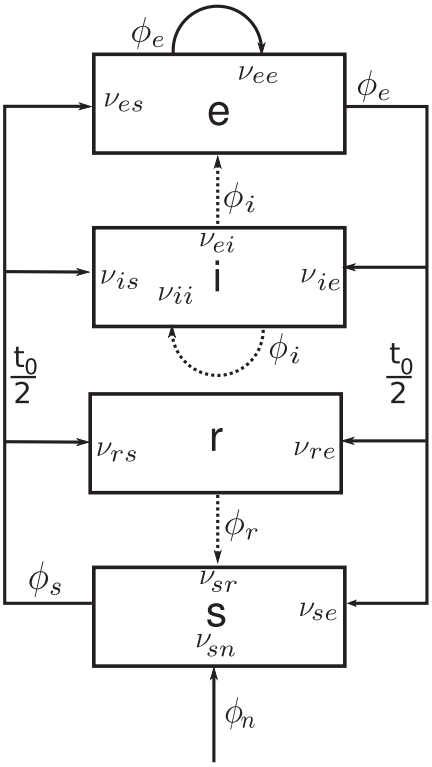

Fig. 1. Schematic diagram of the corticothalamic model system. The neural populations shown are cortical excitatory (e), inhibitory (i), thalamic reticular (r), thalamic relay (s), and n = external inputs. The parameter ν_{ab} quantifies the connection to population a from population b. Inhibitory connections are shown with dashed lines.

2.1. Corticothalamic field model

In order to investigate the dynamics of absence seizure, we use the neural field model of the corticothalamic system seen in Fig. 1. The neural populations are denoted as: e = excitatory cortical; i = inhibitory cortical; s = thalamic relay neurons; r = thalamic reticular nucleus; and n = external inputs. The dynamical variables within each neural population a are the local mean cell-body potential V_a, the mean rate of firing at the cell-body Q_a, and the propagating axonal fields ϕ_a. The firing rates Q_a are related to the potentials V_a by the response function

$$Q_a(\mathbf{r},t) = S[V_a(\mathbf{r},t)], \tag{1}$$

where S is a smooth sigmoidal function that increases from 0 to $Q_{\max}$ as V_a increases from $-\infty$ to ∞, with

$$S(V_a) = \frac{Q_{\max}}{1+\exp[-\pi(V_a-\theta)/\sigma\sqrt{3}]}, \tag{2}$$

where θ is the mean neural firing threshold, σ is the standard deviation of this threshold, and $Q_{\max}$ is the maximum firing rate.

In each neural population, firing rates Q_a generate propagating axonal fields ϕ_a that approximately obey the damped wave equation

$$D_a\phi_a(\mathbf{r},t) = Q_a(\mathbf{r},t), \tag{3}$$

where the spatiotemporal differential operator D_a is

$$D_a = \frac{1}{\gamma_a^2}\frac{\partial^2}{\partial t^2} + \frac{2}{\gamma_a}\frac{\partial}{\partial t} + 1 - r_a^2\nabla^2, \tag{4}$$

where $\gamma_a = v_a/r_a$, r_a and v_a are the characteristic range and conduction velocity of axons of type a, and ∇^2 is the Laplacian operator.

The cell-body potential V_a results after postsynaptic potentials have been filtered in the dendritic tree and then summed. For excitatory and inhibitory neurons within the cortex, this is approximated via the second-order delay-differential equation (Robinson et al., 2001)

$$D_\alpha V_a(\mathbf{r},t) = \nu_{ae}\phi_e(\mathbf{r},t) + \nu_{ai}\phi_i(\mathbf{r},t) + \nu_{as}\phi_s(\mathbf{r},t-t_0/2), \quad (5)$$

where $a = e, i$ and

$$D_\alpha = \frac{1}{\alpha\beta}\frac{d^2}{dt^2} + \left(\frac{1}{\alpha}+\frac{1}{\beta}\right)\frac{d}{dt} + 1. \quad (6)$$

The quantities α and β in Eq. (6) are the inverse decay and rise times, respectively, of the cell-body potential produced by an impulse at a dendritic synapse. Note that input from the thalamus to the cortex is delayed in Eq. (5) by a propagation time $t_0/2$. For neurons within the specific and reticular nuclei of the thalamus, it is the input from the cortex that is time delayed, so

$$D_\alpha V_a(\mathbf{r},t) = \nu_{ae}\phi_e(\mathbf{r},t-t_0/2) + \nu_{as}\phi_s(\mathbf{r},t) + \nu_{ar}\phi_r(\mathbf{r},t) + \nu_{an}\phi_n(\mathbf{r},t), \quad (7)$$

where $a = s, r$. The connection strengths are given by $\nu_{ab} = N_{ab}s_{ab}$, where N_{ab} is the mean number of synapses to neurons of type a from type b and s_{ab} is the strength of the response in neurons a to a unit signal from neurons of type b. The final term on the right-hand side of Eq. (7) describes inputs from outside the corticothalamic system.

2.2. Temporal ramping

Synchronous oscillations between neurons are generated and propagated through the coupling of the various neuronal populations. Previous studies have shown that a gradual increase of the coupling strength between the cortex and thalamus, ν_{se}, can drive the system from a stable steady state to a periodic seizure-like oscillations (limit cycle) via a supercritical Hopf bifurcation (Andrew, 1991; Breakspear et al., 2006; Jirsa et al., 2014; Zhao and Robinson, 2015). In this paper, we thus ramp the corticothalamic coupling strength ν_{se} from an initial value ν_0 to a maximum value $\nu_{\max}$ and back over time. We therefore incorporate a temporal variation function into the model in order to vary ν_{se}

$$f(t) = \tan^{-1}\left[\frac{t-t_1}{\Delta}\right] - \tan^{-1}\left[\frac{t-t_2}{\Delta}\right], \quad (8)$$

where t represents continuous time; t_1 is the time at which the first inverse tangent function reaches its zero; t_2 is the time at which the second inverse tangent function reaches its zero; and, Δ is the characteristic rise and decay time. Next, $0 \le f(t) \le \pi$, so we scale the range of $f(t)$, so $\nu_{se}(t)$ ranges between ν_0 and $\nu_{\max}$

$$\nu_{se}(t) = \nu_0 + (\nu_{\max} - \nu_0)\left[\frac{f(t)-f_{\min}}{f_{\max}-f_{\min}}\right], \quad (9)$$

where $f_{\max}$ and $f_{\min}$ are the maximum and minimum values of $f(t)$ for specific values of t_1, t_2, and Δ. An illustration of the resulting profile given by Eq. (9) is shown in Fig. 2(a).

3. Numerical methods

We use *NFTsim* (Sanz-Leon et al., 2018), which is a publicly available software, to solve Eqs. (1)–(7) numerically for the spatially uniform case in which the ∇^2 term in Eq. (4) vanishes. For the spatially uniform case, the whole population responses simultaneously, which is consistent with the primary generalized absence seizures, where oscillations begin simultaneously across the whole cortex. These are delay differential equations, because there is a propagation time delay $t_0/2$ between the different neural populations present in Eqs. (5) and (7). So, for this specific case, *NFTsim* uses a standard fourth-order Runge–Kutta integration method to solve these equations with a time step dt of 10^{-4} s.

We use the parameters in Table 1 as the initial parameters, which are taken from (Breakspear et al., 2006), with the exception of ν_{se} which we set to $\nu_0 = 1$ mV s, at the start for every simulation. Thus, we do not repeat the value of ν_0 in the remainder of the text. For the set of parameter values mentioned before, the corticothalamic system only has one stable steady state at low firing rates representing normal waking states (Breakspear et al., 2006; Robinson et al., 2002). Indeed, extensive comparisons with experiment have demonstrated that the normal brain operates close to stable fixed points (Abeysuriya et al., 2014a; 2015; 2014b; Breakspear et al., 2006; Chiang et al., 2011; Rennie et al., 2002; Robinson et al., 2002; 2004; 2005). Note that because of the delay time $t_0/2$, these initial steady state conditions are specified for times $-t_0/2 < t \leqslant 0$.

The temporal evolution of ν_{se} is given by Eqs (8) and (9) and depends of three parameters: The maximum connection strength $\nu_{\max}$, characteristic rise time Δ, and characteristic duration $t_2 - t_1$. Thus, to investigate the effect of the variation of $\nu_{\max}$, we ramp up ν_{se} from ν_0 to $\nu_{\max}$ by setting $t_1 = 100$ s, $t_2 = 200$ s, and $\Delta = 10$ s. The maximum connection strength $\nu_{\max}$ is varied from 2.5 mV s to 6.2 mV s. To investigate the effects of the variation of $t_2 - t_1$, we set $\nu_{\max} = 6$ mV s, and $\Delta = 10$ s. The characteristic duration, $t_2 - t_1$ is varied from 75 s to 125 s. Finally, to investigate the effects of the variation of Δ, we set $\nu_{\max} = 6$ mV s, $t_1 = 100$ s, and $t_2 = 200$ s, with a variation of Δ from 10 s to 50 s. A constant input $\phi_n = 2$ s^{-1} is given and no external noise is used for the simulation. Simulations are made 300 s long. We record timeseries every 5 ms. For the dynamic spectrum and power spectrum analysis, we employ the FFT (fast Fourier transform) algorithm with a Hanning window of 600 data points with an overlap of 200 points and sampling frequency of 200 Hz.

4. Seizure dynamics

In this section, we first describe the general characteristics of a generalized absence seizure elicited by the corticothalamic system under a temporal variation of ν_{se} (Section 4.1). Based on the observations from the previous subsection, Section 4.2 introduces an analytically derived approximation to predict the transition time from the pre-ictal state (steady state dynamics) to the ictal state (limit cycle dynamics). Next, in Section 4.3, we analyze the limit-cycle dynamics of each of the corticothalamic populations. Finally, in Sections 4.4–4.6, we present a detailed investigation of the effects of changes in the temporal evolution of ν_{se} on the model seizure dynamics by varying the maximum connection strength $\nu_{\max}$; characteristic rise time Δ; and characteristic duration $t_2 - t_1$, respectively.

4.1. General characteristics

The general characteristics of the dynamics of a model absence seizure onset and offset are illustrated in Figs. 2(a)–(h).

Fig. 2(a) shows the temporal variation of ν_{se}. In this diagram, we distinguish three different regions based on the rate of change of ν_{se} and its sign: Region I from 50 – 125 s, is the rising period in which $\nu_{se}(t-dt) < \nu_{se}(t) < \nu_{\max}$, and thus the rate of change $d\nu_{se}/dt$ is positive and it reaches its maximum at t_1. Region II from 125 – 175 s is the plateau period in which ν_{se} reaches its maximum value and $d\nu_{se}/dt \simeq 0$. Lastly, Region III from 175 – 250 s, is the decaying period in which the rate of change $d\nu_{se}/dt$ is negative and reaches its maximum decaying value at t_2. These regions have

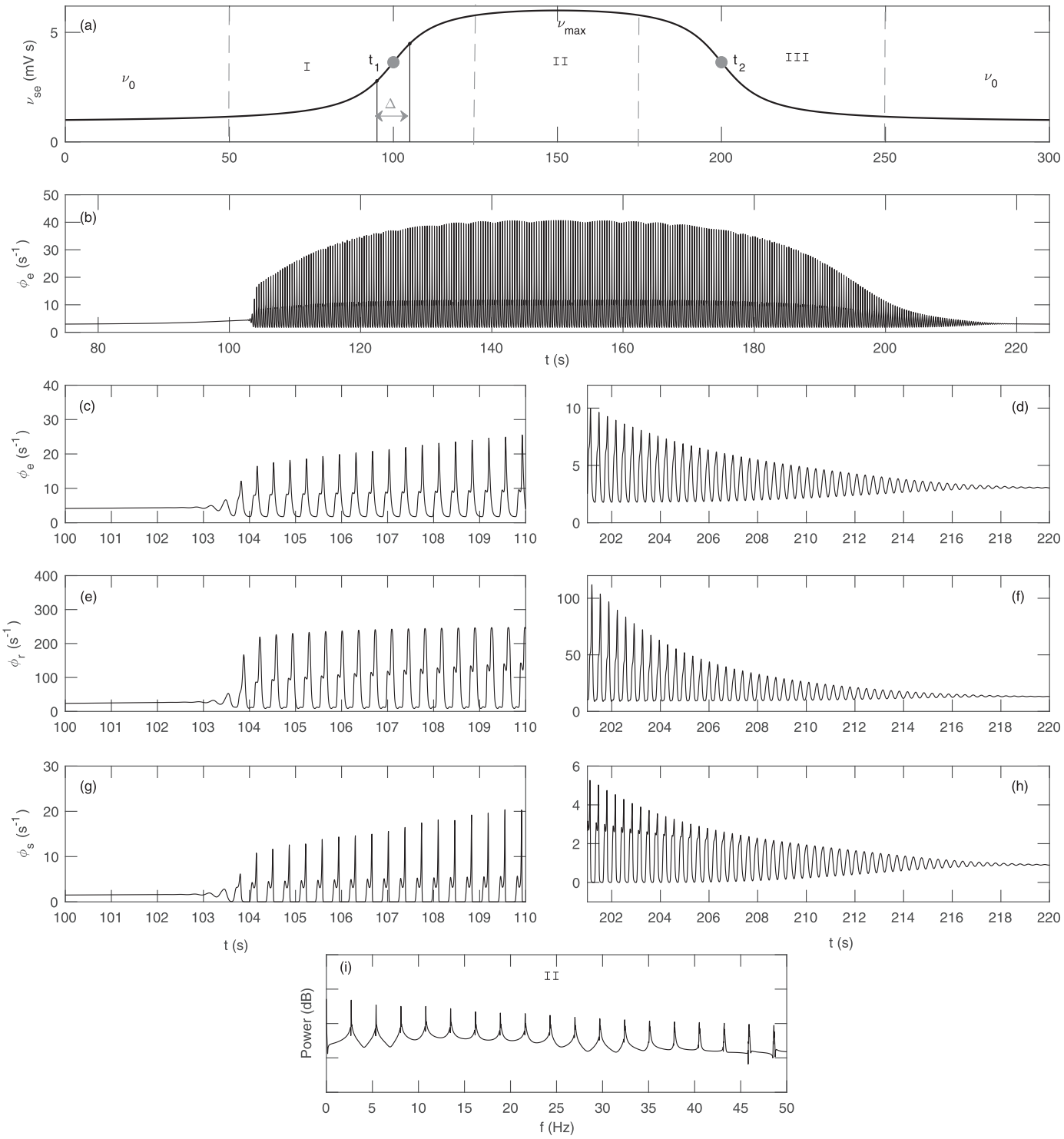

Fig. 2. Corticothalamic dynamics for temporally varying ν_{se}, with $\nu_{\max} = 6$ mV s, $t_1 = 100$ s, $t_2 = 200$ s, $\Delta = 10$ s, and rest of the parameters as in Table 1. (a) Temporal profile of ν_{se} varying from ν_0 to $\nu_{\max}$ and back. Three different regions are identified as: I = rising period, II = plateau period, and III = decaying period. (b) Cortical excitatory field ϕ_e vs. t, showing a $\sim$3 Hz spike-wave oscillation. (c) Zoom of ϕ_e at seizure onset. (d) Zoom of ϕ_e at seizure offset. (e) Time series of ϕ_r at seizure onset. (f) Time series of ϕ_r at seizure offset. (g) Time series of ϕ_s at seizure onset. (h) Time series of ϕ_s at seizure offset. (i) Power spectrum of ϕ_e in Region II. An arbitrary dB scaling is used to normalize the power because clinical EEG recordings involve an additional attenuation by structures between the cortex and the electrode, which we do not model here.

a fixed width and are used in the remainder of the text to analyze different segments of the corticothalamic fields with respect to variations of $\nu_{se}(t)$.

Fig. 2(b) shows the time series of ϕ_e. A sudden appearance of oscillations is seen in this figure at $t \approx 102.2$ s. The system transitions rapidly to a periodically oscillating state from a stable steady state as ν_{se} increases, and then returns smoothly to the same stable steady state as ν_{se} decreases. The transition to periodic dynamics is via a supercritical Hopf bifurcation (Breakspear et al., 2006) for $\nu_{se} \approx 1.8$ mV s, while the SWDs develop for $\nu_{se} \geq 3.4$ mV s

Table 1
Parameters of neural field model of (Breakspear et al., 2006).

Parameter	Value	Unit	Meaning
ν_{ee}, ν_{ie}	1.0	mV s	Excitatory corticocortical connectivity
ν_{ei}, ν_{ii}	−1.8	mV s	Inhibitory corticocortical connectivity
ν_{es}, ν_{is}	3.2	mV s	Specific thalamic to cortical connectivity
ν_{re}	1.6	mV s	Cortical to thalamic reticular connectivity
ν_{rs}	0.6	mV s	Specific to reticular thalamic connectivity
ν_{se}	4.4	mV s	Cortical to specific thalamic connectivity
ν_{sr}	−0.8	mV s	Reticular to specific thalamic connectivity
$\nu_{sn}\phi_n$	2.0	mV	Subthalamic input onto specific thalamus
$Q_{\max}$	250	s^{-1}	Maximum firing rate
θ	15	mV	Mean neuronal threshold
σ	6	mV	Threshold standard deviation
γ_e	100	s^{-1}	Ratio of conduction velocity to mean range of axons
α	50	s^{-1}	Decay rate of membrane potential
β	200	s^{-1}	Rise rate of membrane potential
t_0	80	ms	Corticothalamic return time (complete loop)

(Breakspear et al., 2006). The SWDs are consistent with the spike-wave oscillations of the EEG of absence seizures (Breakspear et al., 2006; Robinson et al., 2002).

A zoom around the seizure onset presented in Fig. 2(c), shows that periodic oscillations of growing amplitude appear in ϕ_e, are shortly followed by the appearance of SWDs which become more prominent with time. The growth of the amplitude of the oscillations is very rapid until the spike-wave oscillations appear, then gradually saturates as ν_{se} increases and reaches $\nu_{\max}$.

Fig. 2(d) shows a zoom around seizure offset, where the system returns to the resting equilibrium state after oscillations damp away, consistent with the behavior of a supercritical Hopf bifurcation (Breakspear et al., 2006). The damping away of the oscillations is more gradual than the appearance of the oscillations in Fig. 2(c). A close zoom also reveals the disappearance of spike-wave discharges well before the oscillations vanish. This dissimilarity between the onset and offset oscillations pattern, which arises because the system bifurcates from a different stable state during onset and offset, is accentuated by the long $t_2 - t_1$ and a slow ramp rate Δ used in for this case. An additional test case with $t_2 - t_1 = 14$ s and $\Delta = 2$ s shows a much symmetric pattern like the one presented in Fig. 3(b) of Breakspear et al. (2006). However, the asymmetry between offset and onset is still present. In Breakspear et al. (2006), a small, yet evident, dissimilarity in the onset and offset pattern can be seen in modeled time series and clinical EEG time series showed in Figs 3(d)-3(e), 4(a) and 4(b), respectively.

Fig. 2(e) shows the time series of ϕ_r for seizure onset. It again shows the spike-wave oscillations like Fig. 2(c). From this plot, it can be seen that $\phi_r \approx 10\phi_e$ during seizure. The secondary wave spikes are also more prominent than those for ϕ_e. A very small peak can be detected in the valleys of the waves, in accord with previous results (Breakspear et al., 2006; Schiff et al., 1995). We study these small peaks in more detail in Section 4.3.

Fig. 2(f) shows the time series of ϕ_r for seizure offset, which exhibits a gradual decrease of the envelope with several sinusoidal oscillations in the tail. The oscillations damp away nearly at the same time as they do for ϕ_e, but the amplitudes are larger.

Fig. 2(g) shows the time series for ϕ_s during seizure onset. Here, we observe that the thalamic field of the specific nuclei is smaller than ϕ_r, but nearly equal to ϕ_e. In addition, the secondary wave peaks are more prominent than those of the ϕ_e and ϕ_r, but the width of the waves is smaller than that of ϕ_e and ϕ_r.

Fig. 2(h) shows the time series of ϕ_s for seizure offset. The oscillations damp away as for ϕ_e and ϕ_r. The specific thalamic field also has a smaller value than ϕ_e and ϕ_r at seizure offset. These outcomes coincide with the observations of Breakspear et al. (2006), except that in this example we explore seizure dynamics in a longer time scale and for a higher $\nu_{\max}$. If we use the $t_2 - t_1 = 14$ s, $\Delta = 2$ s, and $\nu_{\max} = 5.3$ mV s, we can exactly replicate the results and figures of Breakspear et al. (2006) despite the slight changes in the smoothness the temporal evolution of ν_{se}.

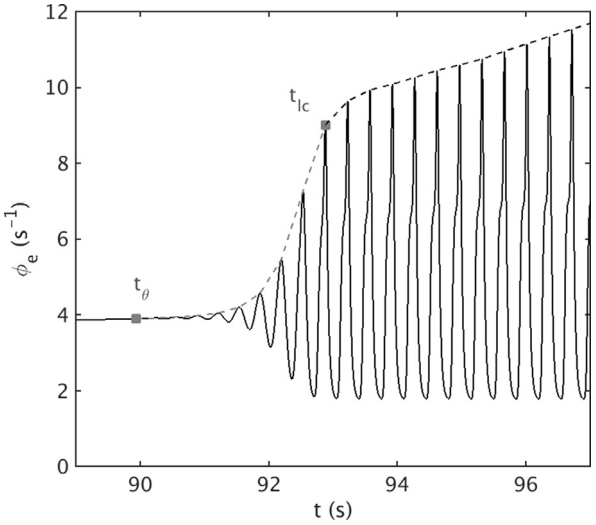

Fig. 3. An overview of seizure onset of the time series of ϕ_e, with $\nu_{\max} = 6$ mV s, $t_2 - t_1 = 100$ s, $\Delta = 30$ s, and rest of the parameters as in Table 1. The gray squares indicate (i) the threshold time, t_θ, at which oscillations start; and, (ii) the time at which the first spike-wave discharge occurs, t_{lc}. The gray dashed line represents the upper envelope of the oscillations during the characteristic time $t_{lc} - t_\theta$. The black dashed line represents the upper envelope of the SWDs amplitude which grow in amplitude for $t > t_{lc}$ until reaching a maximum.

Finally, Fig. 2(i) displays the normalized power spectra of ϕ_e in Region II as defined in Fig. 2(a). As expected, multiple harmonics of ~ 3 Hz seizure oscillations are present in the power spectrum, and their power decreases steadily with increasing frequency.

4.2. Analytic prediction of transition time from pre-ictal state to spike-wave oscillations

In this section we predict the characteristic time required by corticothalamic system to develop spike-wave discharges after $\nu_{se}(t)$ crosses a threshold enough to initialize periodic oscillations.

In the following paragraphs the characteristic time is analytically approximated as a function of (i) the amplitude of the upper envelope of the oscillations A; and, (ii) the rate of change of ν_{se}

$$t_{lc} - t_\theta = f(A(t), \mathrm{d}\nu/\mathrm{dt}), \tag{10}$$

where t_θ is the time at which the first oscillation cycle starts as illustrated in Fig. 3; and t_{lc} is the time at which the highest peak of first SWD occurs, whose amplitude we denote with A_{lc}. Also, we use the following substitutions $\nu_\theta \equiv \nu_{se}(t = t_\theta)$ and $A_\theta \equiv A(t = t_\theta)$, to denote the value of the corticothalamic strength and the amplitude of the oscillations at the threshold time.

If we assume that the rapid-increase phase after crossing ν_θ is dominated by the leading term in the normal form of the equations for a stable supercritical Hopf bifurcation, i.e., $dA/dt = \beta A$, where $\beta \propto \nu_t - \nu_\theta$, the growth of the oscillations amplitude A can be approximated as

$$\frac{\mathrm{d}A}{\mathrm{d}t} \approx C[\nu(t) - \nu_\theta]A, \tag{11}$$

where C is a constant, $\nu(t)$ is the instantaneous value of ν_{se} and ν_θ is the threshold value.

Because ν_{se} only varies with time t, we can make the approximation, $\nu(t) - \nu_\theta \propto t - t_\theta$ near the threshold, when the oscillation starts at A_θ.

$$\frac{dA}{dt} = c(t - t_\theta)A, \tag{12}$$

whose solution is

$$A = A_\theta \exp\left[\frac{c(t - t_\theta)^2}{2}\right]. \tag{13}$$

Next, dividing both terms by A_θ

$$\frac{A}{A_\theta} = \exp\left[\frac{c(t - t_\theta)^2}{2}\right], \tag{14}$$

where $c = Cd\nu(t)/dt|_{t=t_\theta}$ is a constant; we then find for $t = t_{lc}$

$$\exp\left[\frac{c(t_{lc} - t_\theta)^2}{2}\right] = \frac{A_{lc}}{A_\theta}, \tag{15}$$

$$t_{lc} - t_\theta = \sqrt{\frac{2}{c}\ln\left(\frac{A_{lc}}{A_\theta}\right)}, \tag{16}$$

$$t_{lc} - t_\theta = \frac{k}{\sqrt{d\nu(t)/dt|_{t=t_\theta}}}, \tag{17}$$

where $k = [(2/C)\ln(A_{lc}/A_\theta)]^{1/2}$ is a constant and independent of $d\nu(t)/dt|_{t=t_\theta}$. So, the characteristic time from the start of the periodic oscillations to the first spike-wave oscillation can be approximated as

$$t_{lc} - t_\theta \propto \frac{k}{\sqrt{d\nu_{se}/dt}}; \tag{18}$$

and it is inversely proportional to the square root of the rate of change of ν_{se}.

4.3. Characteristics of spike-wave oscillations

To analyze the difference in the limit cycle dynamics of the fields ϕ_e, ϕ_r, and ϕ_s presented in Section 4.1, we plot a few cycles of the SWDs and the trajectories of limit cycle dynamics on the phase space defined by $d\phi_a/dt$ vs ϕ_a. Fig. 4(a) shows the time series of ϕ_e from $t = 149.5$ s to $t = 150.5$ s, which is in Region II when $\nu_{se} \approx \nu_{\max}$. The two peaks discussed previously are very prominent. We indicate the peaks of the cycle around $t = 150$ s with the letters P and R, while the letters Q and S show the minimums. Fig. 4(b) shows the trajectories phase space for the indicated wave. We see the trajectory starts from S, has a loop between P and Q, then returns to S via R.

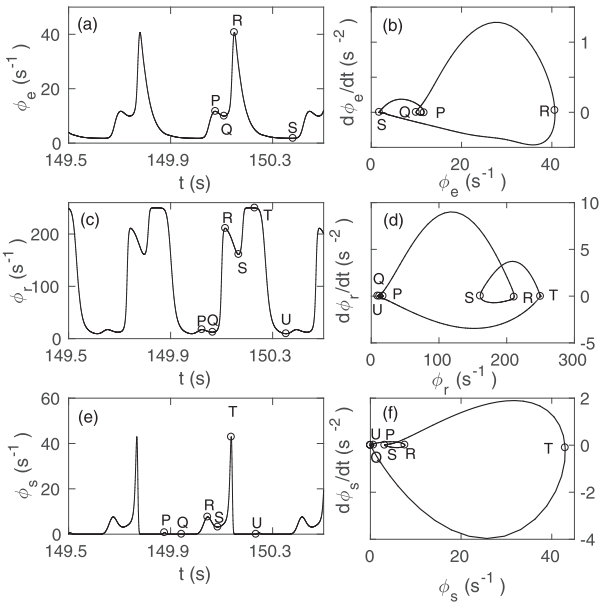

Fig. 4. Limit cycle dynamics of three different fields at $\nu_{se} \approx \nu_{\max}$ and $t \approx 150$ s with $\nu_{\max} = 6$ mV s, $t_2 - t_1 = 100$ s, $\Delta = 10$ s, and rest of the parameters as in Table 1. (a) Close zoom of ϕ_e. (b) Phase space trajectory of ϕ_e for a single wave at $t \approx 150$ s. In (a) and (b), P is the first maximum, Q is the first minimum, R is the second maximum, and S is the second minimum. (c) Close zoom of ϕ_r. (d) Trajectory of ϕ_r. In (c) and (d), P is the first maximum, Q is the first minimum, R is the second maximum, S is the second minimum, T is the third maximum and finally, U corresponds to the third minimum. (e) Close zoom of ϕ_s and (f) trajectory of ϕ_s. For this last two figures P, Q, R, S, T, and U follow the same order of maximums and minimums as the previous ones.

Fig. 4(c) shows the time series of ϕ_r for $t = 149.5 - 150.5$ s. The cycle around $t = 150$ s is marked with six points. Point P corresponds to the first wave peak, Q to the first minimum, R to the second peak and S to the second minimum, T to the third peak, and finally, U to the start of the next cycle. The alignments of the peaks of the waves have a $t_0/2$ time shift from ϕ_e, due to the propagation delay between the different population. A $\phi_r(t)$ vs. $\phi_e(t - t_0/2)$ graph will show the waves with same alignment. This happens because the signal needs $t_0/2$ to reach from cortex to reticular thalamus. The phase space for this wave is given in Fig. 4(d). A limit cycle with three peaks is seen in this figure. The amplitude of peak P is very small compared to the peaks R and T. The amplitude of peak T is the biggest. The relative difference between the amplitudes of the two largest peaks of ϕ_r is also less than that for ϕ_e.

Fig. 4(e) shows the time series of ϕ_s for $t = 149.5 - 151.5$ s. The cycle around $t = 150$ s is again labeled with the six points P, Q, R, S, T, and U as in Fig. 4(c). The phase space for this wave is shown in Fig. 4(f). It is seen that ϕ_s also has a third peak similar to ϕ_r. However, the amplitudes of the peaks are much smaller than ϕ_r. The width of the first and second peaks are also less than that of ϕ_r. The alignment of the peaks and minimums of the waves for ϕ_s is slightly forward than that of ϕ_r.

The phase space trajectory of ϕ_s is very similar to that of ϕ_e, except the appearance of the third small peak at point U. Both ϕ_e and ϕ_s have their highest values nearly at the same time, but the amplitude of the second highest ϕ_s peak is smaller than that of ϕ_e. The alignments of the waves of ϕ_s also have a time delay relative to ϕ_e, because the signal needs $t_0/2$ s to reach from cortex to thalamus and thalamus to cortex.

A close examination of Fig. 4 reveals the mechanism of a signal flowing through the populations. A peak from ϕ_e reaches at ϕ_r and ϕ_s simultaneously approximately 40 ms later. A positive excitation

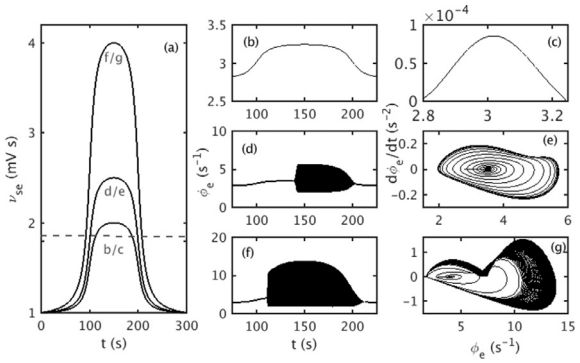

Fig. 5. Effects of ν_{max} on seizure dynamics. (a) Profiles of ν_{se} for $\nu_{max} = 2, 2.5,$ and 4 mV s with $t_2 - t_1 = 100$ s, $\Delta = 10$ s, and other parameters as in Table 1. Labels refer to subsequent pairs of figures. Dashed line corresponds to the seizure threshold. (b) Field for $\nu_{max} = 2$ mV s. (c) Phase space trajectory for $\nu_{max} = 2$ mV s. (d) Field for $\nu_{max} = 2.5$ mV s. Note that individual oscillations are not distinguishable on this scale. (e) Trajectory for $\nu_{max} = 2.5$ mV s. (f) Field for $\nu_{max} = 4$ mV s. (g) Trajectory for $\nu_{max} = 4$ mV s.

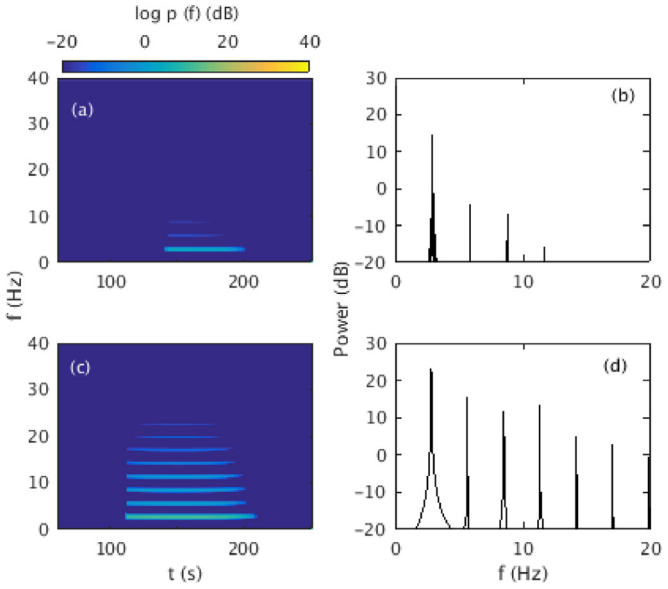

Fig. 6. Spectral variations for different ν_{max} with $t_2 - t_1 = 100$ s, $\Delta = 10$ s, and rest of the parameters showing in Table 1. The power density of the harmonics is calculated for frequencies in between 0–20 Hz and power in between −20–30 dB. A Hanning window of 600 data points with an overlap of 200 points and sampling frequency of 200 Hz was used for the spectrogram. Color bar shows the dB scale of the power spectrum. (a) Dynamic spectrum for $\nu_{max} = 2.5$ mV s. (b) Average spectrum for $\nu_{max} = 2.5$ mV s. (c) Dynamic spectrum for $\nu_{max} = 4$ mV s. (d) Average spectrum for $\nu_{max} = 4$ mV s.

of ϕ_r appears immediately, which suppresses ϕ_s. This suppression then influences ϕ_e 40 ms later. As a result, a negative perturbation to ϕ_e is generated at the cortex, which then flows to the thalamus again. By this time, ϕ_r has decreased in the absence of inputs. A period of near silence in all three fields is reached at that point. After a further time 40 ms, the negative signal from ϕ_e reaches the thalamus and generates a negative excitation of ϕ_r, which allows a positive excitation of ϕ_s. This positive excitation then flows to ϕ_e and initializes the next cycle of the loop. This morphology is also consistent with Breakspear et al. (2006).

4.4. Variation of maximum connection strength

Fig. 5(a) shows the effect of varying the maximum connection strength from $\nu_{max} = 2$ mV s to $\nu_{max} = 6.5$ mV s, with fixed $t_2 - t_1 = 100$ s, $\Delta = 10$ s, and rest of the parameters as in Table 1.

Fig. 5(b) and (c) present time series and trajectories of ϕ_e for $\nu_{max} = 2$ mV s, respectively. It is seen that ϕ_e gradually increases with ν_{se} until $\nu_{se} = \nu_{max}$, then gradually returns to its initial value when ν_{se} returns to ν_0. No oscillations are developed in this case.

Fig. 5(d) shows time series of ϕ_e for $\nu_{max} = 2.5$ mV s, which is enough to initiate periodic oscillations in the system but with a lower firing rate than for higher ν_{max}. Fig. 5(e) is the phase space diagram for $\nu_{max} = 2.5$ mV s. An unstable fixed point is seen to spiral outward with a growing amplitude until it reaches onto the limit cycle attractor. This region corresponds to the left half of Fig. 5(d), when ν_{se} is ramped up to ν_{max} from ν_0. When ν_{se} returns to ν_0, the orbit decays on the same manifold.

A dominant spike-wave oscillation is observed from the time series of ϕ_e for $\nu_{max} = 4$ mV s in Fig. 5(f). The oscillations are seen to start much earlier before ν_{se} reaches its plateau value $\nu_{max} = 2.5$ mV s, because the system crosses the threshold earlier for greater ν_{max}. Fig. 5(g) shows the phase space diagram for $\nu_{max} = 4$ mV s. A stable limit cycle oscillation with a greater amplitude is seen in this figure. The small second loop on the limit cycle represents the second spike with a smaller amplitude. This second spike was absent in the phase space diagram of $\nu_{max} = 2.5$ mV s. The amplitudes of the small loops, which correspond to the small spikes remain equal for all ν_{max} values. The amplitude of ϕ_e is found to increase with increasing ν_{max}. However, when $\nu_{se} > 6.2$ mV s, we find that the system does not return to its initial resting state when ν_{se} returns to ν_0 because system settles to another stable steady state at $\phi_e \approx Q_{max}$.

The dynamic spectrum and power spectrum of the harmonics that have peak power above −20 dB are shown in Fig. 6. Fig. 6(a) shows the dynamic power spectrum for $\nu_{max} = 2.5$ mV s. During seizure we observe a frequency peak $f \approx 3$ Hz in the spectrum, consistent with the characteristic frequency of absence seizures. Fig. 6(b) shows the average power spectrum from 125 s to 175 s for $\nu_{max} = 2.5$ mV s. Three harmonics are observed above −20 dB in this figure, but the second and third are much weaker than fundamental. Fig. 6(c) shows the dynamic power spectrum for $\nu_{max} = 4$ mV s; multiple harmonics are seen in this figure. Fig. 6(d) shows the average power spectrum for $\nu_{max} = 4$ mV s, showing that both the number of intense harmonics and their power increase for $\nu_{max} = 4$ mV s.

From Fig. 6(a) and (c), it is seen that the number of intense harmonics increases with ν_{max}, as do the duration above −20 dB and the spectral width and power of the harmonics. A broadening of the frequency during the seizure onset due to the rapid change of connection strength for higher ν_{max} is also observed in these figures. Fig. 6(b) and (d) show that the amplitude of the harmonics increases with ν_{max}. However, close examination shows that the limit cycle frequency decreases as ν_{max} increases; e.g., the first harmonic frequency drops from 2.93 Hz to 2.70 Hz as ν_{max} increases from 2.5 mV s to 6 mV s, consistent with large limit cycles taking longer to traverse. An initial drop in frequency is seen, with additional broadening due to the sudden seizure onset. An opposite feature is seen at seizure termination. A small increase in frequency is seen due to the sudden seizure offset.

Fig. 7 shows the effects of the variation of ν_{max} on the system. Fig. 7(a) shows that ϕ_{max}, which is the maximum amplitude of ϕ_e, increases with ν_{max}. Fig. 7(b) plots the powers of the harmonics for different ν_{max}, showing an increase of the power with ν_{max}. The number of harmonics above −20 dB is seen to increase and the duration of these harmonics also increases with ν_{max} because the system stays above threshold longer.

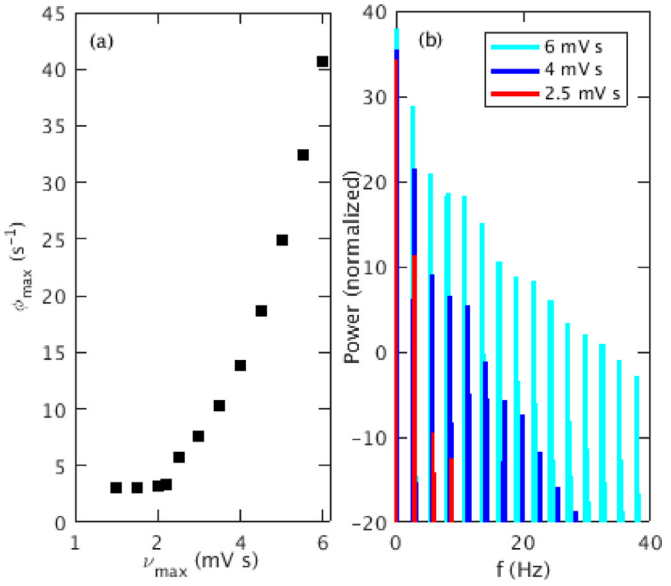

Fig. 7. Effects of the variation of $\nu_{\max}$ with $t_2 - t_1 = 100$ s, $\Delta = 10$ s, and other parameters as in Table 1. (a) Change of maximum firing rate with $\nu_{\max}$. (b) Power spectrum for different $\nu_{\max}$. Legend shows corresponding values of $\nu_{\max}$.

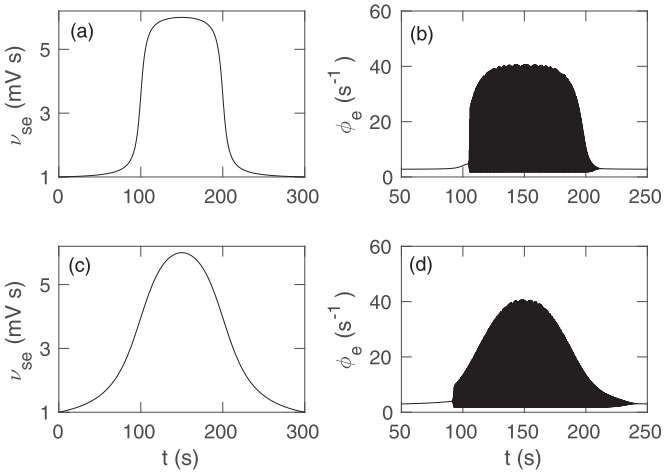

Fig. 8. Effects of Δ on seizure dynamics with $\nu_{\max} = 6$ mV s, $t_2 - t_1 = 100$ s, and other parameters as in Table 1. (a) Profile of ν_{se} for $\Delta = 5$ s. (b) Field $\Delta = 5$ s. (c) Profile for $\Delta = 30$ s and (d) field $\Delta = 30$ s. Individual oscillations cannot be distinguished on this scale.

4.5. Variation of ramp rate

Variation of ramp rate is done by changing Δ in Eq. (8), with a large Δ corresponding to a slow rate of change of ν_{se}. In order to see the effects of Δ, we fix $\nu_{\max} = 6$ mV s, $t_2 - t_1 = 100$ s, and rest of the parameters as in Table 1.

Fig. 8 show the effects of Δ on the time series of ϕ_e. Figures (a) and (b) show the profile of ν_{se} and the time series of ϕ_e for $\Delta = 5$ s, respectively. Figures (c) and (d) show the profile of ν_{se} and time series of ϕ_e for $\Delta = 30$ s, respectively. It is seen the oscillations start earlier for greater Δ as the system crosses the bifurcation earlier. A zoomed view of the time series of ϕ_e for $\Delta = 30$ s has been shown in Fig. 3, in which it can be observed that the amplitudes of the oscillations increase very rapidly at the beginning. This fast increase corresponds to a short characteristic transition time as defined by Eq. (18). On the other hand, the characteristic time for $\Delta = 30$ s would be much longer.

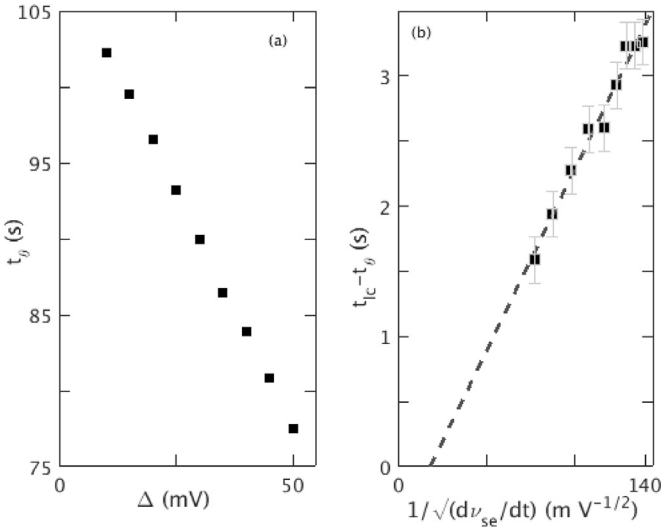

Fig. 9. Effects of the variation of Δ with $\nu_{\max} = 6$ mV s, $t_2 - t_1 = 100$ s, and rest of the parameters as in Table 1. (a) Seizure threshold, t_θ, vs. Δ. (b) Time $t_{lc} - t_\theta$ to go to the limit cycle oscillations from threshold, vs. $(d\nu_{se}/dt)^{-1/2}$.

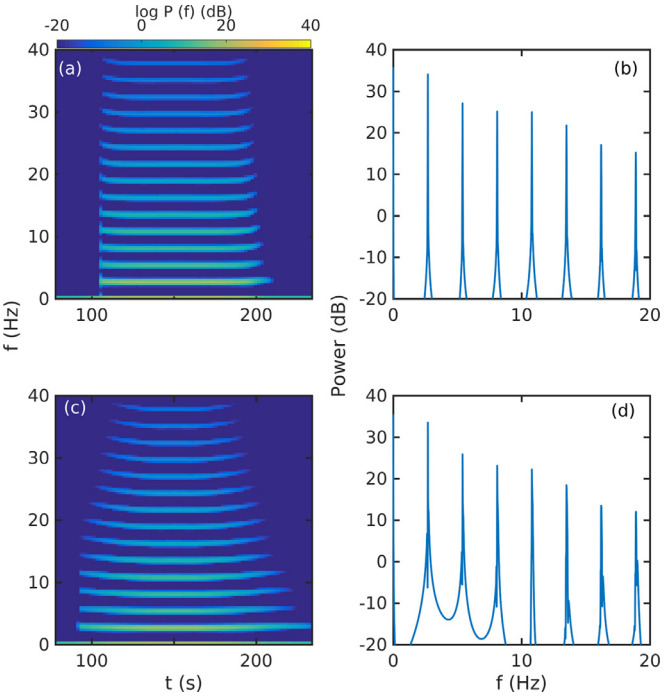

Fig. 10. Frequency spectrums in the ictal (125–175 s) states for different Δ with $\nu_{\max} = 6$ mV s, $t_2 - t_1 = 100$ s, and rest of the parameters as in Table 1. Color bar shows dB scale of the power spectrum. (a) Dynamic spectrum for $\Delta = 5$ s. (b) Average spectrum for $\Delta = 5$ s. (c) Dynamic spectrum for $\Delta = 30$ s. (d) Average spectrum for $\Delta = 30$ s.

We show the change of t_θ with Δ in Fig. 9(a) to verify Eq. (18). It is seen that the oscillations indeed start earlier for large Δ. Fig. 9(b) shows $t_{lc} - t_\theta$ vs. $(d\nu_{ab}/dt)^{-1/2}$; a least-squares fit yields

$$t_{lc} - t_\theta = (0.028 \pm 0.002)(d\nu_{se}/dt)^{-\frac{1}{2}} - (0.2 \pm 0.2), \qquad (19)$$

which is consistent with Eq. (18).

Dynamic spectrograms and average power spectra for different Δ are shown in Fig. 10. Fig. 10(a) and (b) show the dynamic spectrogram and average power spectrum for $\Delta = 5$ s, respectively. Fig. 10(c) and (d) show the dynamic spectrogram and average power spectrum for $\Delta = 30$ s, respectively. From Fig. 10(a)

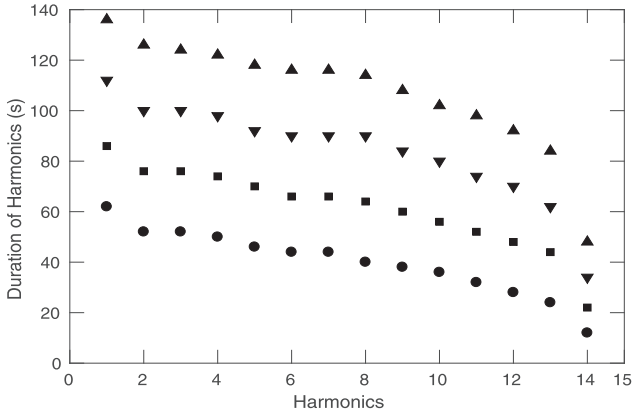

Fig. 11. Effects of $t_2 - t_1$ on the durations of the harmonics seen in the spectrogram with peak power greater than −20 dB with $\nu_{\max} = 6$ mV s, $\Delta = 10$ s, and other parameters as in Table 1. Round dots are the durations of the oscillations for $t_2 - t_1 = 50$ s. Squares are for $t_2 - t_1 = 75$ s. Downward pointing triangles are for $t_2 - t_1 = 200$ s and upward pointing triangles for $t_2 = 225$ s.

and (c), it is seen that for a higher Δ, which corresponds to a lower ramp rate, the duration of the oscillations increases. This is because, for greater Δ and fixed $\nu_{\max}$ and $t_2 - t_1$, the system reaches the threshold earlier. Which causes the system to spend more time above the threshold; hence, the system gets more time to develop oscillations before transitioning to SWDs. However, the durations of higher harmonics are greater for lower Δ and decrease sharply with increasing Δ. The frequency drop from the seizure onset to the limit cycle oscillation also increases with increasing Δ. Fig. 10(b) and (d), show that the power of the harmonics decreases slightly with increasing Δ.

4.6. Effects of characteristic duration

By keeping t_1 constant and changing t_2, we can vary the seizure duration. We examine the dynamics of ϕ_e for several cases ranges from $t_2 - t_1 = 15$ s to 125 s in order to see the effects of the variation of $t_2 - t_1$ on seizure dynamics by fixing $\nu_{\max} = 5.3$ mV s, $\nu_0 = 1$ mV s, $\Delta = 10$ s, and rest of the parameters as in Table 1. Increasing $t_2 - t_1$ implies increasing the time spent above threshold, which as a result will increase the duration of the oscillating period. Fig. 11 shows the impact of the variation of $t_2 - t_1$ on the duration of the harmonics seen in the frequency spectrum. It is seen that the durations of the harmonics increase with $t_2 - t_1$. We also find that decreasing $t_2 - t_1$ decreases the asymmetry in the spiking oscillation pattern seen in Fig. 2(c) and (d) for seizure onset and offset, respectively. Spectral analysis also showed that the power of the frequency peaks increases slightly with $t_2 - t_1$. However, we find that maximum firing rates are unaffected by the ramp duration, so long as there is time for the limit cycle to become fully established, and the seizure oscillations start at the same value of ν_{se}. Despite the variation of the duration of the harmonics, the limit cycle frequencies are also identical for all cases related to a higher value of $\nu_{\max}$. However $t_2 - t_1$ has significant impact on the system with a small $\nu_{\max}$. Fig. 12 shows an example of such system with $\nu_{\max} = 2.2$ mV s, $\Delta = 10$ s, and rest of the parameters as in Table 1. Fig. 12(a) shows the time series of ϕ_e for $t_2 - t_1 = 50$ s. No oscillation is seen in this figure. Fig. 12(b) shows the time series for $t_2 - t_1 = 100$ s. In this figure, a ~ 3 Hz oscillation with a very small power of ~ -30 dB is seen for a very short period of time. Fig. 12(c) shows the time series of ϕ_e for $t_2 - t_1 = 150$ s. Here we see a prominent ~ 3 Hz spike wave oscillation with a power of ~ 9.4 dB. Hence, for a smaller $\nu_{\max}$, seizure like dynamics can be introduced by a greater $t_2 - t_1$.

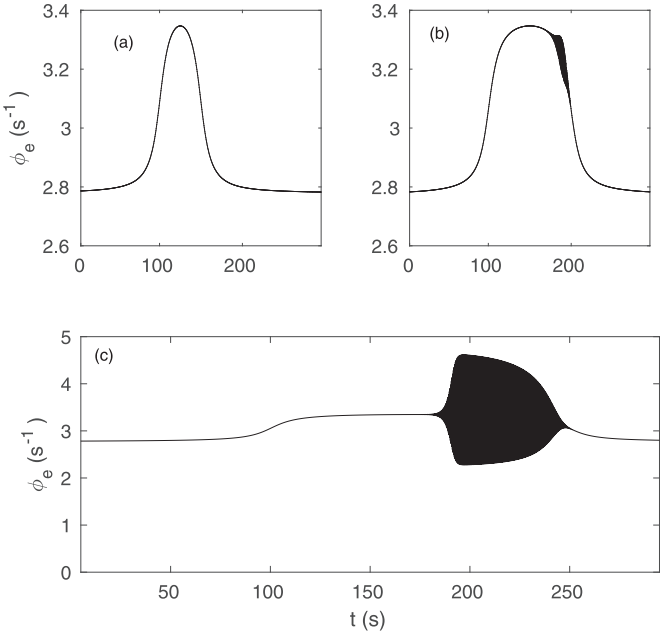

Fig. 12. Time series for different characteristic durations $t_2 - t_1$ with $\nu_{\max} = 2.2$ mV s, $\Delta = 10$ s and parameters in Table 1. (a) ϕ_e vs. t for $t_2 - t_1 = 50$ s. (b) ϕ_e vs. t for $t_2 - t_1 = 100$ s, and (c) ϕ_e vs. t for $t_2 - t_1 = 150$ s.

5. Summary

We have used an established neural field model of the corticothalamic system (Breakspear et al., 2006; Zhao and Robinson, 2015) along with a temporally varying connection strength between the cortex and the thalamus in order to study the dependence of model absence seizures on a physiological connection strength and its time course. Specifically, we investigated spectral and temporal characteristics of seizures by varying the maximum height, duration, and ramp rate of the coupling strength. Using these outcomes, it is also possible to qualitatively predict the effects of varying other connection strengths because they will exhibit similar dynamics due to the universality properties of the Hopf bifurcation. The key outcomes are:

(i) The system exhibits a ~ 3 Hz limit cycle oscillation once the connection strength crosses the bifurcation threshold, which is the characteristic frequency of absence seizures. This is consistent with previous studies that showed that increasing the corticothalamic connection strength beyond a threshold can push the system into the seizure state via a supercritical Hopf bifurcation (Breakspear et al., 2006; Marten et al., 2009; Robinson et al., 2002; Zhao and Robinson, 2015). The system can be returned to the resting equilibrium by decreasing the connection strength below the threshold. However, in cases with $\nu_{\max} \gtrsim 6.2$ mV s, the corticothalamic system may settle in a steady state close to $Q_{\max}$.

(ii) The maximum amplitude ϕ_e reaches during oscillatory dynamics mostly depends on the maximum connection strength, $\nu_{\max}$. Increasing $\nu_{\max}$ also increases the firing rate because an increase of the connectivity strength increases the strength of the negative feedback loop between the cortex and the thalamus and the amplitude of limit cycle.

(iii) Because the maximum connection strength increases the amplitudes of the non-sinusoidal limit cycle oscillations, increasing the maximum connection strength increases the power of the harmonics as well as the characteristic number of harmonics. The frequency drop of the limit cycle fre-

quency from the onset also decreases with the increasing $\nu_{\max}$.

(iv) An increase of $\nu_{\max}$ increases the total duration of the seizure because the system reaches threshold earlier and stays longer above the threshold for greater $\nu_{\max}$.

(v) Oscillations start earlier for a longer ramp time Δ, because the system crosses the threshold earlier. The total duration of the seizure increases with Δ, because the system remains above threshold longer. The average power of the harmonics also decreases slightly with Δ.

(vi) The characteristic time required to reach spike-wave oscillations from the start of oscillatory activity is predicted to be inversely proportional to the square root of the rate of change of the connection strength. A linear fit to numerical results confirms this prediction. Using Eq. (18), one can predict the temporal scales at which underlying physiological parameters operate in order to trigger and suppress absence seizures.

(vii) Increasing the characteristic duration $t_2 - t_1$ above threshold increases the total duration of the oscillations. It also increases the power of the harmonics slightly.

(Viii) The characteristic duration $t_2 - t_1$ do not have significant impacts on the wave properties of ϕ_e useless the temporal profile has small amplitude. For a small $\nu_{\max}$, it is possible to reduce the amplitude and the strength of the seizure oscillations by reducing $t_2 - t_1$.

Overall, the present study enables the spectral and temporal characteristics of model seizures to be related to underlying physiological variations and makes a range of specific, testable predictions, as summarized in the preceding points. The neural field model we used, has been successfully used by several authors to reproduced and unified many observed features of brain activity, including seizures (Abeysuriya et al., 2014a; 2015; van Albada et al., 2010; Breakspear et al., 2006; 2003; Kim and Robinson, 2007; Marten et al., 2009; O'Connor and Robinson, 2004; Rennie et al., 2002; Roberts and Robinson, 2008; Robinson, 2006; Robinson et al., 2002; 2004; 2001; 2003; Rodrigues et al., 2006; Zhao and Robinson, 2015). Previous studies also showed the quantitative comparison of the prediction of this model about seizure with the real EEG data (Breakspear et al., 2006). Hence, the outcomes can also be used for potential clinical applications, such as explaining the variability of seizure onset across subjects by examining the temporal and spectral characteristics of seizure. By comparing the amplitudes of the frequency peaks or the phase diagram of the patient with our analysis, it will be possible to constrain the magnitude of the connection strength during a seizure. By comparing the duration, number, and the width of the harmonics of the patient with our spectrograms it is also possible to find the duration above the threshold, and the rate of change of the corticothalamic connection strength. Because the connection strength is also a function of time, the study of the variation of amplitudes of clinical EEG with time and the relation we found here between the maximum connection strength and the amplitude, will let us map the change of connection strength during the seizure.

The better understanding of the effects of magnitude, duration, and rate of change of the connection strength between the thalamus and the cortex of the patient will be helpful to understand the physiology from the wave-spike characteristics. A better approximation of the physiological properties of the connection strength will be helpful to potentially inform seizure control strategies (Schiff, 2012).

Acknowledgments

This work was supported by the Australian Research Council Center of Excellence Grant CE140100007, and by Australian Research Council Laureate Fellowship Grant FL140100025.

References

Abeysuriya, R.G., Rennie, C.J., Robinson, P.A., 2014a. Prediction and verification of nonlinear sleep spindle harmonic oscillations. J. Theor. Biol. 344, 70–77.
Abeysuriya, R.G., Rennie, C.J., Robinson, P.A., 2015. Physiologically based arousal state estimation and dynamics. J. Neurosci. Methods 253, 55–69.
Abeysuriya, R.G., Rennie, C.J., Robinson, P.A., Kim, J.W., 2014b. Experimental observation of a theoretically predicted nonlinear sleep spindle harmonic in human eeg. Clin. Neurophysiol. 125 (10), 2016–2023.
van Albada, S.J., Kerr, C.C., Chiang, A.K.I., Rennie, C.J., Robinson, P.A., 2010. Neurophysiological changes with age probed by inverse modeling of eeg spectra. Clin. Neurophysiol. 121 (1), 21–38.
Andrew, R.D., 1991. Seizure and acute osmotic change: clinical and neurophysiological aspects. J. Neurol. Sci. 101 (1), 7–18.
Berényi, A., Belluscio, M., Mao, D., Buzsáki, G., 2012. Closed-loop control of epilepsy by transcranial electrical stimulation. Science 337 (6095), 735–737.
Breakspear, M., 2017. Dynamic models of large-scale brain activity. Nat. Neurosci. 20 (3), 340.
Breakspear, M., Roberts, J.A., Terry, J.R., Rodrigues, S., Mahant, N., Robinson, P.A., 2006. A unifying explanation of primary generalized seizures through nonlinear brain modeling and bifurcation analysis. Cerebral Cortex 16 (9), 1296–1313.
Breakspear, M., Terry, J.R., Friston, K.J., 2003. Modulation of excitatory synaptic coupling facilitates synchronization and complex dynamics in a biophysical model of neuronal dynamics. Netw. Comput. Neural Syst. 14 (4), 703–732.
Browne, T.R., Holmes, G.L., 2000. Handbook of Epilepsy. Lippincott Williams & Wilkins, Philadelphia.
Chen, M., Guo, D., Wang, T., Jing, W., Xia, Y., Xu, P., Luo, C., Valdes-Sosa, P.A., Yao, D., 2014. Bidirectional control of absence seizures by the basal ganglia: a computational evidence. PLoS Comput. Biol. 10 (3), e1003495.
Chiang, A.K.I., Rennie, C.J., Robinson, P.A., van Albada, S.J., Kerr, C.C., 2011. Age trends and sex differences of alpha rhythms including split alpha peaks. Clin. Neurophysiol. 122 (8), 1505–1517.
Coombes, S., Terry, J.R., 2012. The dynamics of neurological disease: integrating computational, experimental and clinical neuroscience. Eur. J.Neurosci. 36 (2), 2118–2120.
Crunelli, V., Leresche, N., 2002. Childhood absence epilepsy: genes, channels, neurons and networks. Nat. Rev. Neurosci. 3 (5), 371–382.
Deco, G., Jirsa, V.K., Robinson, P.A., Breakspear, M., Friston, K.J., 2008. The dynamic brain: from spiking neurons to neural masses and cortical fields. PLoS Comput. Biol. 4 (8), e1000092.
Destexhe, A., 1999. Can gabaa conductances explain the fast oscillation frequency of absence seizures in rodents? Eur. J. Neurosci. 11 (6), 2175–2181.
Dhamala, M., Jirsa, V.K., Ding, M., 2004. Transitions to synchrony in coupled bursting neurons. Phys. Rev. Lett. 92 (2), 028101.
Engel, J., Pedley, T.A., 1997. Epilepsy: A Comprehensive Textbook, 1. Lippincott-Raven, Philadelphia.
Freeman, W.J., 1975. Mass Action in the Nervous System. Academic Press, New York.
Godlevsky, L.S., Kobolev, E.V., van Luijtelaar, E.L.J.M., Coenen, A.M.L., Stepanenko, K.I., Smirnov, I.V., 2006. Influence of transcranial magnetic stimulation on spike-wave discharges in a genetic model of absence epilepsy. Indian J. Exp. Biol. 44, 949–954.
Guye, M., Regis, J., Tamura, M., Wendling, F., Gonigal, A.M., Chauvel, P., Bartolomei, F., 2006. The role of corticothalamic coupling in human temporal lobe epilepsy. Brain 129 (7), 1917–1928.
Hall, D., Kuhlmann, L., 2013. Mechanisms of seizure propagation in 2-dimensional centre-surround recurrent networks. PLoS ONE 8 (8), e71369.
Jirsa, V.K., Haken, H., 1996. Field theory of electromagnetic brain activity. Phys. Rev. Lett. 77 (5), 960–963.
Jirsa, V.K., Proix, T., Perdikis, D., Woodman, M.M., Wang, H., Gonzalez-Martinez, J., Bernard, C., Bénar, C., Guye, M., Chauvel, P., Bartolomei, F., 2017. The virtual epileptic patient: individualized whole-brain models of epilepsy spread. Neuroimage 145, 377–388.
Jirsa, V.K., Stacey, W.C., Quilichini, P.P., Ivanov, A.I., Bernard, C., 2014. On the nature of seizure dynamics. Brain 137 (8), 2210–2230.
Kim, J.W., Roberts, J.A., Robinson, P.A., 2009. Dynamics of epileptic seizures: evolution, spreading, and suppression. J. Theor. Biol. 257 (4), 527–532.
Kim, J.W., Robinson, P.A., 2007. Compact dynamical model of brain activity. Phys. Rev. E 75 (3), 031907.
Kramer, M.A., Truccolo, W., Eden, U.T., Lepage, K.Q., Hochberg, L.R., Eskandar, E.N., Madsen, J.R., Lee, J.W., Maheshwari, A., Halgren, E., Chu, C.J., Cash, S.S., 2012. Human seizures self-terminate across spatial scales via a critical transition. Proc. Natl. Acad. Sci. 109 (51), 21116–21121.
Larter, R., Speelman, B., Worth, R.M., 1999. A coupled ordinary differential equation lattice model for the simulation of epileptic seizures. Chaos 9 (3), 795–804.
Liley, D.T.J., Bojak, I., 2005. Understanding the transition to seizure by modeling the epileptiform activity of general anesthetic agents. J. Clin. Neurophysiol. 22 (5), 300–313.

Liley, D.T.J., Cadusch, P.J., Wright, J.J., 1999. A continuum theory of electro-cortical activity. Neurocomputing 26, 795–800.
van Luijtelaar, G., Lüttjohann, A., Makarov, V.V., Maksimenko, V.A., Koronovskii, A.A., Hramov, A.E., 2016. Methods of automated absence seizure detection, interference by stimulation, and possibilities for prediction in genetic absence models. J. Neurosci. Methods 260, 144–158.
Lopes da Silva, F.H., Pijn, J.P., Velis, D., Nijssen, P.C.G., 1997. Alpha rhythms: noise, dynamics and models. Int. J. Psychophysiol. 26 (1), 237–249.
Luo, C., Li, Q., Xia, Y., Lei, X., Xue, K., Yao, Z., Lai, Y., Martı, E., Liao, W., Zhou, D., Valdes-Sosa, P.A., Gong, Q., Yao, D., 2012. Resting state basal ganglia network in idiopathic generalized epilepsy. Hum. Brain Mapp. 33 (6), 1279–1294.
Lytton, W.W., 2008. Computer modelling of epilepsy. Nat. Rev. Neurosci. 9 (8), 626–637.
Lytton, W.W., Orman, R., Stewart, M., 2005. Computer simulation of epilepsy: implications for seizure spread and behavioral dysfunction. Epilepsy Behav. 7 (3), 336–344.
Marten, F., Rodrigues, S., Benjamin, O., Richardson, M.P., Terry, J.R., 2009. Onset of polyspike complexes in a mean-field model of human electroencephalography and its application to absence epilepsy. Philos. Trans. R. Soc. London A 367 (1891), 1145–1161.
Meeren, H.K.M., Pijn, J.P.M., van Luijtelaar, E.L.J.M., Coenen, A.M.L., Lopes da Silva, F.H., 2002. Cortical focus drives widespread corticothalamic networks during spontaneous absence seizures in rats. J. Neurosci. 22 (4), 1480–1495.
Nunez, P.L., 1974. The brain wave equation: a model for the eeg. Math. Biosci. 21 (3–4), 279–297.
O'Connor, S.C., Robinson, P.A., 2004. Spatially uniform and nonuniform analyses of electroencephalographic dynamics, with application to the topography of the alpha rhythm. Phys. Rev. E 70 (1), 011911.
Panayiotopoulos, C.P., 1999. Typical absence seizures and their treatment. Arch. Dis. Child. 81 (4), 351–355.
Penfield, W., 1933. The evidence for a cerebral vascular mechanism in epilepsy. Ann. Intern. Med. 7 (1–6), 303–310.
Pinotsis, D.A., Moran, R.J., Friston, K.J., 2012. Dynamic causal modeling with neural fields. Neuroimage 59 (2), 1261–1274.
Prevett, M.C., Duncan, J.S., Jones, T., Fish, D.R., Brooks, D.J., 1995. Demonstration of thalarnic activation during typical absence seizures using h2 15o and pet. Neurology 45 (7), 1396–1402.
Proix, T., Bartolomei, F., Chauvel, P., Bernard, C., Jirsa, V.K., 2014. Permittivity coupling across brain regions determines seizure recruitment in partial epilepsy. J. Neurosci. 34 (45), 15009–15021.
Rennie, C.J., Robinson, P.A., Wright, J.J., 2002. Unified neurophysical model of eeg spectra and evoked potentials. Biol. Cybern. 86 (6), 457–471.
Roberts, J.A., Robinson, P.A., 2008. Modeling absence seizure dynamics: implications for basic mechanisms and measurement of thalamocortical and corticothalamic latencies. J. Theor. Biol. 253 (1), 189–201.
Robinson, P.A., 2006. Patchy propagators, brain dynamics, and the generation of spatially structured gamma oscillations. Phys. Rev. E 73 (4), 041904.
Robinson, P.A., Rennie, C.J., Rowe, D.L., 2002. Dynamics of large-scale brain activity in normal arousal states and epileptic seizures. Phys. Rev. E 65 (4), 041924.
Robinson, P.A., Rennie, C.J., Rowe, D.L., O'connor, S.C., 2004. Estimation of multiscale neurophysiologic parameters by electroencephalographic means. Hum. Brain Mapp. 23 (1), 53–72.
Robinson, P.A., Rennie, C.J., Rowe, D.L., O'Connor, S.C., Gordon, E., 2005. Multiscale brain modelling. Philos. Trans. R. Soc. B 360 (1457), 1043–1050.
Robinson, P.A., Rennie, C.J., Wright, J.J., 1997. Propagation and stability of waves of electrical activity in the cerebral cortex. Phys. Rev. E 56 (1), 826.
Robinson, P.A., Rennie, C.J., Wright, J.J., Bahramali, H., Gordon, E., Rowe, D.L., 2001. Prediction of electroencephalographic spectra from neurophysiology. Phys. Rev. E 63 (2), 021903.
Robinson, P.A., Whitehouse, R.W., Rennie, C.J., 2003. Nonuniform corticothalamic continuum model of electroencephalographic spectra with application to split-alpha peaks. Phys. Rev. E 68 (2), 021922.
Rodrigues, S., Barton, D., Szalai, R., Benjamin, O., Richardson, M.P., Terry, J.R., 2009. Transitions to spike-wave oscillations and epileptic dynamics in a human cortico-thalamic mean-field model. J. Comput. Neurosci. 27 (3), 507–526.
Rodrigues, S., Terry, J.R., Breakspear, M., 2006. On the genesis of spike-wave oscillations in a mean-field model of human thalamic and corticothalamic dynamics. Phys. Lett. A 355 (4–5), 352–357.
Salek-Haddadi, A., Diehl, B., Hamandi, K., Merschhemke, M., Liston, A., Friston, K., Duncan, J.S., Fish, D.R., Lemieux, L., 2006. Hemodynamic correlates of epileptiform discharges: an eeg-fmri study of 63 patients with focal epilepsy. Brain Res. 1088 (1), 148–166.
Sanz-Leon, P., Robinson, P.A., Knock, S.A., Drysdale, P.M., Abeysuriya, R.G., Fung, P.K., Rennie, C.J., Zhao, X., 2018. NFTSim: theory and simulation of multiscale neural field dynamics. (Under Review) PLoS Comput. Biol.
Schiff, N.D., Victor, J.D., Canel, A., Labar, D.R., 1995. Characteristic nonlinearities of the 3/s ictal electroencephalogram identified by nonlinear autoregressive analysis. Biol. Cybern. 72 (6), 519–526.
Schiff, S.J., 2012. Neural Control Engineering: The Emerging Intersection Between Control Theory and Neuroscience. MIT Press, Cambridge.
Seidenbecher, T., Staak, R., Pape, H.C., 1998. Relations between cortical and thalamic cellular activities during absence seizures in rats. Eur. J. Neurosci. 10 (3), 1103–1112.
Steriade, M., Amzica, F., Neckelmann, D., Timofeev, I., 1998. Spike-wave complexes and fast components of cortically generated seizures. ii. extra-and intracellular patterns. J. Neurophysiol. 80 (3), 1456–1479.
Steriade, M., Contreras, D., 1998. Spike-wave complexes and fast components of cortically generated seizures. i. role of neocortex and thalamus. J. Neurophysiol. 80 (3), 1439–1455.
Suffczynski, P., Kalitzin, S., Lopes da Silva, F.H., 2004. Dynamics of non-convulsive epileptic phenomena modeled by a bistable neuronal network. Neuroscience 126 (2), 467–484.
Suffczynski, P., Lopes da Silva, F.H., Parra, J., Velis, D., Kalitzin, S., 2005. Epileptic transitions: model predictions and experimental validation. J. Clin. Neurophysiol. 22 (5), 288–299.
Tan, H.O., Reid, C.A., Single, F.N., Davies, P.J., Chiu, C., Murphy, S., Clarke, A.L., Dibbens, L., Krestel, H., Mulley, J.C., Jones, M.V., Seeburg, P.H., Sakmann, B., Berkovic, S.F., Sprengel, R., Petrou, S., 2007. Reduced cortical inhibition in a mouse model of familial childhood absence epilepsy. Proc. Natl. Acad. Sci. 104 (44), 17536–17541.
Ullah, G., Wei, Y., Dahlem, M.A., Wechselberger, M., Schiff, S.J., 2015. The role of cell volume in the dynamics of seizure, spreading depression, and anoxic depolarization. PLoS Comput. Biol. 11 (8), e1004414.
Velazquez, J.L.P., Dominguez, L.G., Gaetz, W., Cheyne, D., Snead III, O.C., Wennberg, R., 2006. Fluctuations in phase synchronization in brain activity: physiological interpretations of phase locking patterns. Topical Problems of Nonlinear Wave Physics. International Society for Optics and Photonics. 597510–597510
Vercueil, L., Benazzouz, A., Deransart, C., Bressand, K., Marescaux, C., Depaulis, A., Benabid, A.L., 1998. High-frequency stimulation of the sub-thalamic nucleus suppresses absence seizures in the rat: comparison with neurotoxic lesions. Epilepsy Res. 31 (1), 39–46.
Vergnes, M., Marescaux, C., 1992. Cortical and thalamic lesions in rats with genetic absence epilepsy.. J. Neural Transm. 35, 71–83.
Voss, L.J., Jacobson, G., Sleigh, J.W., Steyn-Ross, A., Steyn-Ross, M., 2009. Excitatory effects of gap junction blockers on cerebral cortex seizure-like activity in rats and mice. Epilepsia 50 (8), 1971–1978.
Wallace, R.H., Marini, C., Petrou, S., Harkin, L.A., Bowser, D.N., Panchal, R.G., Williams, D.A., Sutherland, G.R., Mulley, J.C., Scheffer, I.E., Berkovic, S.F., 2001. Mutant gaba a receptor γ2-subunit in childhood absence epilepsy and febrile seizures. Nat. Genet. 28 (1), 49–52.
Wendling, F., 2008. Computational models of epileptic activity: a bridge between observation and pathophysiological interpretation. Expert Rev. Neurother. 8 (6), 889–896.
Wendling, F., Hernandez, A., Bellanger, J.J., Chauvel, P., Bartolomei, F., 2005. Interictal to ictal transition in human temporal lobe epilepsy: insights from a computational model of intracerebral eeg. J. Clin. Neurophysiol. 22 (5), 343–356.
Williams, D., 1953. A study of thalamic and cortical rhythms in petit mal. Brain 76 (1), 50–69.
Yang, D.P., Robinson, P.A., 2017. Critical dynamics of hopf bifurcations in the corticothalamic system: transitions from normal arousal states to epileptic seizures. Phys. Rev. E 95 (4), 042410.
Zhao, X., Robinson, P.A., 2015. Generalized seizures in a neural field model with bursting dynamics. J. Comput. Neurosci. 39 (2), 197–216.